




Active external control effect on the collective locomotion of two tandem self-propelled flapping plates

Cite as: Phys. Fluids **33**, 101901 (2021); <https://doi.org/10.1063/5.0065256>

Submitted: 31 July 2021 • Accepted: 10 September 2021 • Published Online: 04 October 2021

 Linlin Kang (康林林),  Ze-Rui Peng (彭泽瑞),  Haibo Huang (黄海波), et al.



View Online



Export Citation



CrossMark

ARTICLES YOU MAY BE INTERESTED IN

[Flow map of foil undergoing combined fast and slow pitching](#)

Physics of Fluids **33**, 101902 (2021); <https://doi.org/10.1063/5.0063992>

[Hydrodynamics of a fish-like body undulation mechanism: Scaling laws and regimes for vortex wake modes](#)

Physics of Fluids **33**, 101904 (2021); <https://doi.org/10.1063/5.0062304>

[Body-caudal fin fish-inspired self-propulsion study on burst-and-coast and continuous swimming of a hydrofoil model](#)

Physics of Fluids **33**, 091905 (2021); <https://doi.org/10.1063/5.0061417>

LEARN MORE

 Author Services

Maximize your publication potential with
English language editing and
translation services



Active external control effect on the collective locomotion of two tandem self-propelled flapping plates

Cite as: Phys. Fluids **33**, 101901 (2021); doi: [10.1063/5.0065256](https://doi.org/10.1063/5.0065256)

Submitted: 31 July 2021 · Accepted: 10 September 2021 ·

Published Online: 4 October 2021



View Online



Export Citation



CrossMark

Linlin Kang (康林林),^{1,a)}  Ze-Rui Peng (彭泽瑞),²  Haibo Huang (黄海波),³  Xi-Yun Lu (陆夕云),^{3,b)} 
and Weicheng Cui (崔维成)^{1,a),c)} 

AFFILIATIONS

¹Key Laboratory of Coastal Environment and Resources of Zhejiang Province (KLaCER), School of Engineering, Westlake University, Hangzhou 310024, Zhejiang, China

²Department of Mechanics, School of Aerospace Engineering, Huazhong University of Science and Technology, Wuhan 430074, China

³Department of Modern Mechanics, University of Science and Technology of China, Hefei 230026, Anhui, China

^{a)}Also at: Institute of Advanced Technology, Westlake Institute for Advanced Study, Hangzhou 310024, Zhejiang, China.

^{b)}Electronic mail: xlu@ustc.edu.cn

^{c)}Author to whom correspondence should be addressed: cuiweicheng@westlake.edu.cn

ABSTRACT

The self-organization of active swimmers is interesting but not fully understood. Lighthill conjectured that the orderly configurations may emerge passively from the hydrodynamic interactions rather than active control mechanism. To further test Lighthill's conjecture, the effect of active control on the propulsive performance of two self-propelled flapping plates in tandem configuration is studied. Different types of external horizontal forces are applied at the leading edge of the following plate. It is found that the collective dynamic and propulsive performance of the two-plate system are mainly affected by the mean value of the external horizontal force rather than its specific form. The two-plate self-propelled system has certain ability to counteract a limited external intervention and maintain the orderly configuration by adjusting the gap spacing between two plates. For a stable configuration, the external intervention hardly affects the propulsion velocity but has a significant monotonic effect on the gap spacing and input work. Further, a simplified model is proposed to relate the external horizontal force to the gap spacing between two plates and verified to be reliable by the numerical results. Moreover, the momentum and energy transferred to fluid are investigated in terms of local vortical structures. It is revealed that the impulse of the wake vortex pair is hardly affected by the external horizontal force, while its kinetic energy and the local dissipative energy vary monotonically with it. These results may shed some light on the understanding of collective behaviors of living swimmers and robotic fish.

Published under an exclusive license by AIP Publishing. <https://doi.org/10.1063/5.0065256>

I. INTRODUCTION

Collective behaviors of large aggregations of animals exist widely in nature.¹ Particularly interesting is that a large number of synchronized active bodies self-organize into orderly patterns, like insect swarms,² fish schools,^{3,4} and bird flocks.⁵ The investigations of collective motion can bring new ideas to the research of evolutionary biology,⁶ fluid engineering,⁷ swarm intelligence,⁸ and other fields, so it has been a hot topic. Apart from the social traits, such as foraging and defense from predators,⁹ the most quoted function of collective motion is to extract energy from the surrounding fluid and enhance propulsive performance through flow interactions.^{4,10,11} Consequently,

the role of hydrodynamics in collective motion has received considerable attention for several decades, but some issues remain open.¹²

One intriguing and important issue is the role of flow in the emergent self-organizing behavior of collective locomotion. Weihs used a two-dimensional inviscid model to predict that fish swimming diagonally behind the upstream fish would particularly benefit from the vortices shed by the upstream fish.³ The vortices help to drag the following fish forward. The question arises whether passive hydrodynamic forces bring the orderly configurations into play or whether very elaborate control mechanisms act to maintain the orderly collective pattern. Lighthill conjectured that the orderly configuration is

generated passively and spontaneously due to the hydrodynamic effect.¹³ His conjecture seems to have not been experimentally or numerically tested or observed until recent years.^{12,14,15}

The experiments of directly observing the collective motions of living fish and birds can reveal some fundamental characteristics and mechanisms of fish schools,⁴ bird flocks,⁵ or fish moving through vortex street.¹⁰ However, there are some constraints in experimental studies of living animals in terms of operability and measurability. For example, the kinematic motions of living animals are difficult to control, and the force and power are hard to measure.¹⁶ Numerical or experimental simulation of a simplified multi-body self-propelled system is an effective approach to study the hydrodynamic role of collective motion of real organisms. Li *et al.*¹⁷ used three-dimensional numerical simulations of a pair of schooling fish, with kinematics and geometry obtained from experimental data, to examine their energetics and stability. Li *et al.*¹⁸ developed biomimetic fish-like robots to study the energy consumption associated with swimming together in pairs. There are also some works^{19,20} that model two-dimensional fish-like bodies under a traveling wavy lateral motion to study the hydrodynamic interactions thereof.

Considering the fact that most fish and birds use flapping fins/wings to generate propulsive performance, a more common simplified model for studying the collective motion is two (or more) flapping foils or flexible plates. This approach has been used to study the flow-mediated interactions between passively flapping plates in the oncoming flow^{21–24} as well as active flapping bodies.^{25–28} By fixing the bodies in the oncoming flow, studies show that the force on the follower depends on its interaction with vortices shed by the leader.²⁹ However, these studies of tandem bodies held at fixed streamwise positions with prescribed flapping motions do not account for the feedback of fins/wings to surrounding fluid.

A proven way to study the self-organized collective motion is to allow the bodies free to propel in fluid and dynamically select their speed and gap spacing.^{11,12,14–16,30–35} For example, Zhu *et al.*¹⁴ numerically studied two self-propelled flexible plates swimming in tandem with identical flapping motion. They found that after flapping for several periods, the two plates spontaneously form an equilibrium gap spacing. The gap spacing is about integer multiples of the natural spacing of the vortex streets. Ramanarivo *et al.*¹⁵ found the same phenomenon through experiments of arrays of flapping wings that propel within a collective wake. To address Lighthill's conjecture, they disturbed the follower to deviate from its equilibrium position. They found that the follower is subjected to a restoring force directed to the equilibrium position. This restoring force comes from the fluid. And more recently, Newbolt *et al.*³² and Yu *et al.*²⁰ found that two airfoils with different flapping amplitudes and frequencies can also spontaneously form a stable configuration. Lin *et al.*³⁶ numerically confirmed that two flapping foils can simultaneously converge to equilibrium gap spacings in both lateral and longitudinal directions.

Current studies^{12,14,15} indicate that the self-organization of the collective motion may be formed passively and spontaneously due to the hydrodynamic effect, as Lighthill conjectured. These models all adopted two (or multiple) self-propelled bodies with identical flapping motion, without considering individual active adjustment from pectoral fins or other propulsion modes. However, for actual collectives, individuals within the formation may take the initiative to adjust their own movements in response to changes in the surrounding environment. For example, individuals in the fish schools are known to

influence the foraging behavior of the group and the ability of a school to navigate toward a target,⁹ by actively adjusting their swimming speed/direction, relative positions with neighbors, etc. A variety of collective models have been established to mimic how individual-level movement regulation influences collective behaviors, such as Boids model³⁷ and Vicsek model.¹ In these models, the complex emergent behaviors may arise from the interaction of individual agents adhering to a set of simple rules. These models have achieved great success in capturing global behaviors. However, since the rules applied in the models are artificially set based on phenomenological observations, for the collections of actively moving swimmers in a fluid, the underlying physical mechanism of individual-level actively control regulating group behavior remains unclear and to be studied. It involves an in-depth test of Lighthill's conjecture.

In terms of propulsion modes, the fish swimming styles can usually be put into two major categories, one belongs to the body/caudal fin (BCF) propulsion, where significant “flapping” action occurs only at the caudal fin (producing more than 90% of thrust); the second is the median/paired fin propulsion (MPF) and is achieved by “rowing” movements of pectoral fins.^{38,39} It is estimated that most fish use BCF modes for propulsion and rely on MPF modes for maneuvering and stabilization.⁴⁰ The advantages of these combined swimming modes have inspired the development of man-made underwater devices that integrate multiple propulsion modes for propulsion and maneuvering purposes. For example, Liao *et al.*⁴¹ developed a biomimetic robotic fish that uses an integrated oscillation and jet propulsive mechanism to enable good swimming performance for small robotic fish. Wang *et al.*⁴² formulated a 3D dynamic model for the robotic fish actuated by pectoral and caudal fins which can produce multi-mode swimming. It is seen that both active swimmer and robotic fish typically not only rely on flapping motion to achieve efficient propulsion but also can have some other active control mechanism to achieve maneuvering and stabilization. However, the current simplified models for studying the collective motion only adopt the flapping motion (oscillatory or undulatory), which belongs to the BCF locomotion. To our knowledge, there is no work that studies the effect of active control on the coherence and propulsive performance of collective motion, but it is a question worth investigating. In our simplified model of two tandem self-propelled flapping plates, we study such an active control effect (from the pectoral fins or other propulsion modes) by exerting an external horizontal force on the leading edge of the following plate.

Also as pointed out by Oza *et al.*,⁵³ the influence of hydrodynamics on the self-organization of collection motion has been relatively unexplored theoretically. A common way to understand the mechanism of force generation and energy consumption by flapping plates/foils is to relate them to the vorticity shedding patterns. Given the kinematic motion of the bodies, the generation and evolution of such vorticity distributions depend on unsteady large-scale boundary layer separation. It is difficult to analyze using a simple analytical approach. The complicated physics of vortex shedding remains an obstacle to a quantitative analysis of vortex-body interactions in collective motion. To quantify the influence of local vortical structures on the force of the body, some vorticity-based force expressions are developed,^{43,44} which may shed some light on the understanding the multiple-body/body-vortex interaction problems.

At present, the in-depth testing of Lighthill's conjecture is still lacking. The question arises whether and to what extent stable the orderly

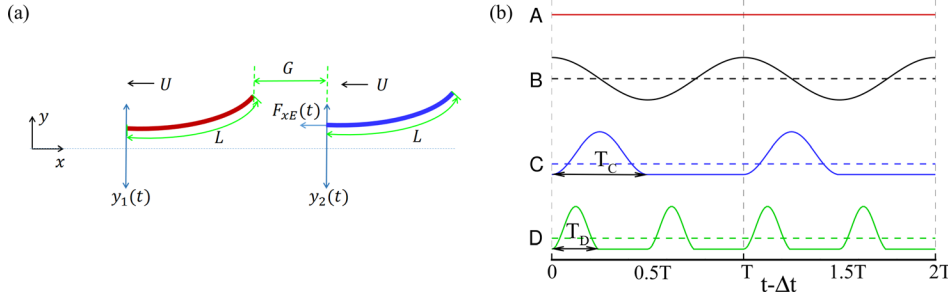


FIG. 1. (a) Schematic diagram for the two self-propelled plates driven by plunging motions in a tandem configuration. G is the gap spacing between the two plates. $F_{xE}e_x$ is an external loading applied at the leading edge of the following plate. y_i is the lateral coordination of the i th plate. L is the length of each plate. U is the propulsion velocity. (b) Schematic diagram of four (A, B, C, D) different types of external horizontal force F_{xE} as a function of time.

configuration is. To address this, inspired by Ramanarivo *et al.*¹⁵ and Peng *et al.*,¹² we consider a particular version of the two tandem self-propelled flapping-plates problem. The plates are driven by harmonic plunging motions of identical frequency and amplitude. Unlike previous works,^{12,14} an external horizontal force is exerted on the leading edge of the following plate. Four types of external horizontal force, which represent active controls of following swimmer in the configurations, are applied in our simulations. The influence of the external horizontal forces on stable orderly pattern and propulsive performance has been systematically investigated. We quantitatively study the momentum and energy transfer in terms of local vortical structures as well.

The rest of the paper is organized as follows. The physical problem, governing equations, and numerical methods are described in Sec. II. The results and discussions regarding the active control effect on the propulsive performance (orderly configuration, swimming speed, input work, etc.) and wake structures are given from a comprehensive numerical and theoretical investigation in Sec. III. The conclusions are summarized in Sec. IV. Finally, the detailed introduction and validation of the present methodology, the derivation of the simplified dynamical model, and some supplementary material for quantitative flow analysis are presented in Appendix A–D.

II. PROBLEM DESCRIPTION AND NUMERICAL METHOD

A. Physical problem and mathematical formulation

As shown in Fig. 1(a), two flapping flexible plates with length L swim in tandem. Each plate is driven at the leading edge by harmonic plunging motion in the lateral direction,

$$y_i(t) = A \cos(2\pi ft), \quad (1)$$

where y_i is the lateral coordination of i th plate ($i = 1, 2$), A and f are the plunging amplitude and frequency, respectively. t is the time. An external loading $F_{xE}e_x$ is exerted on the leading edge of the following plate. The purpose of applying an external horizontal loading is to influence the interactions between the following plate and the wake vortices of the leader. As shown in Fig. 1(b), four functional forms of external horizontal loading $F_{xE}(t)$ are considered (cf. Table I). $T = 1/f$ is the flapping period. F_A, F_{B1}, F_{B2}, F_C and F_D are all constants. $T_C \leq T$ and $T_D \leq T/2$. Force type A denotes a constant external horizontal force. The period of $F_{xE}(t)$ of force types B and C is T , and the period of force type D is $T/2$. Force type B is a harmonic function, which may appear in the rowing motion of the median/paired fin.⁴⁰ Force types C and D are used in place of the step function, which may come from the jet propulsive mechanism;⁴¹ T_C/T and $2T_D/T$ are the duty cycles, which represent the proportion of external force acting time to the flapping cycle. Δt denotes the phase difference between the external horizontal loading $F_{xE}(t)$ and the flapping motion $y_2(t)$.

The fluid motion is described by the incompressible Navier–Stokes equations,

$$\frac{\partial \mathbf{u}}{\partial t} + \mathbf{u} \cdot \nabla \mathbf{u} = -\frac{1}{\rho} \nabla p + \frac{\mu}{\rho} \nabla^2 \mathbf{u} + \mathbf{f}, \quad (2)$$

$$\nabla \cdot \mathbf{u} = 0, \quad (3)$$

where \mathbf{u} is the velocity, p the pressure, ρ the density of fluid, and μ the dynamic viscosity. \mathbf{f} is the Eulerian force acting on the surrounding

TABLE I. Functional forms of external horizontal loading $F_{xE}(t)$ in the simulations.

Force type	Function of $F_{xE}(t)$	Mean value of $F_{xE}(t)$, \bar{F}_{xE}
A	F_A	F_A
B	$F_{B1} + F_{B2} \cdot \cos(2\pi(t - \Delta t)/T)$	F_{B1}
C	$\begin{cases} F_C - F_C \cos(2\pi(t - \Delta t)/T_C), & \frac{(t - \Delta t)}{T} - \lfloor \frac{(t - \Delta t)}{T} \rfloor \leq \frac{T_C}{T}, \\ 0, & \frac{(t - \Delta t)}{T} - \lfloor \frac{(t - \Delta t)}{T} \rfloor > \frac{T_C}{T}. \end{cases}$	$F_C \times T_C/T$
D	$\begin{cases} F_D - F_D \cos(2\pi(t - \Delta t)/T_D), & \frac{2(t - \Delta t)}{T} - \lfloor \frac{2(t - \Delta t)}{T} \rfloor \leq \frac{2T_D}{T}, \\ 0, & \frac{2(t - \Delta t)}{T} - \lfloor \frac{2(t - \Delta t)}{T} \rfloor > \frac{2T_D}{T}. \end{cases}$	$2F_D \times T_D/T$

fluid due to the immersed boundary (IB), as constrained by the velocity boundary condition.

The plates are assumed to be two-dimensional thin elastic beams and their dynamics are governed by the nonlinear partial differential equation,⁴⁵

$$\rho_s h \frac{\partial^2 \mathbf{X}}{\partial t^2} - \frac{\partial}{\partial s} \left[Eh \left(1 - \left| \frac{\partial \mathbf{X}}{\partial s} \right|^{-1} \right) \frac{\partial \mathbf{X}}{\partial s} \right] + EI \frac{\partial^4 \mathbf{X}}{\partial s^4} = \mathbf{F}_s + \mathbf{F}_{ext}, \quad (4)$$

where s is the Lagrangian coordinate along the plate, \mathbf{X} is the position vector of the plate, $\rho_s h$ is the structural linear mass density, Eh and EI are the structural stretching rigidity and bending rigidity, respectively. \mathbf{F}_s is the Lagrangian force exerted on the plates by the surrounding fluid. \mathbf{F}_{ext} ($= F_{x\mathbf{e}_x}$) represents the active control which only acts on the leading edge of the following plate. In addition to satisfying Eq. (1), the leading edge of the plate satisfies boundary conditions $\frac{\partial \mathbf{X}}{\partial s} = \mathbf{e}_x$ and $-Eh \left(1 - \left| \frac{\partial \mathbf{X}}{\partial s} \right|^{-1} \right) \frac{\partial \mathbf{X}}{\partial s} + EI \frac{\partial^3 \mathbf{X}}{\partial s^3} = \mathbf{0}$, where \mathbf{e}_x is the unit vector in the x direction. $-Eh \left(1 - \left| \frac{\partial \mathbf{X}}{\partial s} \right|^{-1} \right) \frac{\partial \mathbf{X}}{\partial s} + EI \frac{\partial^3 \mathbf{X}}{\partial s^3} = \mathbf{0}$ and $\frac{\partial^2 \mathbf{X}}{\partial s^2} = \mathbf{0}$ are imposed at the trailing edge.

The reference quantities L , ρ , and U_{ref} are chosen to nondimensionalize the above mathematical formulation, where U_{ref} is the maximum flapping velocity of the plunging motion, i.e., $U_{ref} = 2\pi Af$. The dimensionless parameters are defined as follows: the heaving amplitude A/L , the Reynolds number $Re = \rho U_{ref} L / \mu$, the bending stiffness $K = EI / \rho U_{ref}^2 L^3$, the stretching stiffness $S = Eh / \rho U_{ref}^2 L$, the mass ratio of the plates $M = \rho_s h / \rho L$ and the gap spacing G/L . In the following descriptions, A and G denote the normalized quantity A/L and G/L .

B. Numerical method

The Navier–Stokes equations are solved numerically by the lattice Boltzmann method (LBM).^{46,47} The deformation and motion of flexible plate are described by structural equation which is solved by a finite element method⁴⁸ in the Lagrange coordinate independently. For each plate, boundary conditions for the leading and trailing ends are imposed. The movement of each plate (Lagrange points) is coupled with the LBM solver through immersed boundary (IB) method. The body force \mathbf{f} in Eq. (2) represents an interaction force between the fluid and the immersed boundary to enforce the no-slip velocity boundary condition, which on the Eulerian points can be obtained from the Lagrangian force \mathbf{F}_s using the Dirac δ function.⁴⁹ See Appendix A for a detailed description of the numerical method. The validations of the numerical method and grid spacing used in the present study are shown in Appendix B.

The above numerical strategy has been successfully applied to a wide range of fluid–structure interaction problems, such as flow over an inverted flexible plate,⁵⁰ locomotion of one or more flexible flapping plates.^{12,51,52} Similar numerical strategy was also independently developed by De Rosi *et al.*,^{53–55} and was also successfully used to study the aeroelastic problem of flexible flapping wings.²⁶

Based on our convergence studies with different computational domains, the computational domain is chosen as $45L \times 30L$ in the x and y direction. The mesh is uniform with spacing $\Delta x = \Delta y = 0.01L$. The time step is $\Delta t/T = 1/10\,000$ with $T = 1/f$ being the flapping period. Such grid spacing and time step can ensure that the Mach number is sufficiently low to reduce deleterious compressibility effects

affecting the solution of the lattice Boltzmann equation (LBE). For example, in our numerical validation case (see Fig. 13 in Appendix B), the Mach number is less than 0.05. A finite moving computational domain is used in the x direction. As the plate travels one mesh spacing in the horizontal direction, the computational domain is shifted by adding one layer at the inlet and removing one layer at the outlet.⁵¹

III. RESULTS AND DISCUSSION

In this paper, the self-organization of two flapping plates swimming in tandem, under the intervention of an active horizontal loading, is investigated numerically and qualitatively. The controlled nondimensional parameters used in the simulations are listed in Table II. Because this paper focuses on the underlying mechanism of self-organization of collective motion rather than the influence laws of different parameters on propulsion performance, only two groups of parameters are selected. Here, the stretching deformation can be ignored, since the stretching stiffness of plate is large enough. The bending stiffness is $O(1)$ which is within the bending stiffness of real fish.⁵¹ Since at $M = 0.2$, an isolated plate with $K = 1$ achieves the maximum cruising speed, the mass ratio is set $M = 0.2$ in our simulation. These parameters are also consistent with case “1A” and case “2A” in Zhu *et al.*,¹⁴ and show reasonably high propulsive performance. For the sake of generality, case 1 and case 2 are of 2P mode (in which two vortices with the same sign are shed within half cycle) and of 2S mode (in which one vortex is shed with in half cycle), respectively.

The previous works^{12,14} indicate that the orderly configurations of two flapping plates swimming in tandem can be categorized into compact configuration and regular configuration. For the former, the two plates are too closer and the vortex-body analysis is not so clear as that in the regular form. Hence, in the present study, we focus on the regular configuration to analyze the effect of active control on the stability and propulsive performance of the two-plate system. For regular configuration, the gap spacing between the plates of in-phase flapping is usually about an integer multiple of the wavelength traced out by the leading plate, $\lambda = \int_{t_0}^{t_0+T} U dt$. It should be noted that, for regular form, although the initial gap spacing and phase difference between two plates affect the equilibrium gap spacing of final stable configuration, they will not affect the relative position of the following plate in the spatial periodic vortex street.¹⁴ The interaction between the following plate and wake vortices of the leader depends only on flapping amplitude, frequency, and active control. Hence, the initial gap spacing and phase difference are not discussed in this paper.

A. The emergence of stable configuration

To explore the mechanism of the orderly formation, Ramanarivoo *et al.*¹⁵ applied an external torque on the following foil

TABLE II. Values of control parameters used in simulations.

Parameters	Case 1	Case 2
Mass ratio, M	0.2	0.2
Heaving amplitude, A	0.5	0.2
Reynolds number, Re	200	200
Bending stiffness, K	0.8	3.0
Stretching stiffness, S	1000	1000

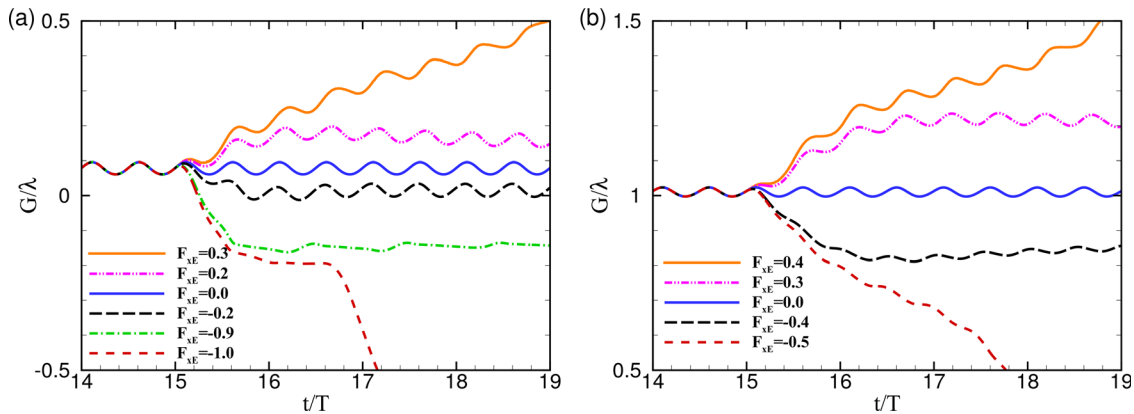


FIG. 2. Gap spacing G as a function of time for case 1 with a constant external horizontal force F_{xE} exerted on the leading edge of the following plate at $t/T = 15$. $\lambda = \int_{t_0}^{t_0+T} U dt$. (a) Compact configuration; (b) regular configuration.

by using a string-mass-pulley system, to make it deviate from its stable position, and they found that the fluid would give a restoring force to the following foil and make it return to its original equilibrium position. Inspired by this work, we apply a time-dependent external horizontal force on the leading edge of the following plate and investigate the propulsive performance of the two-plate self-propulsion system under external force intervention.

To intuitively describe the influence of the active horizontal loading F_{xE} on the evolution of orderly configurations of two plates, Fig. 2 shows the time history of the gap spacing G between two plates for the compact configuration and the regular configuration of case 1, respectively. For both configurations, the plates converge to the stable configurations after flapping for several periods. The equilibrium gap spacings of compact configuration and regular configuration with $F_{xE} = 0$ are about 0.1λ and 1.0λ , respectively. At $t = 15T$, an constant external horizontal force F_{xE} is applied on the leading edge of the following plate, and the gap spacing between two plates starts to change. For $F_{xE} < 0$, the gap spacing will decrease; and for $F_{xE} > 0$, the gap spacing will increase. For the compact configuration, the stable zone is $F_{xE} \in [-0.9, 0.2]$. It means when $F_{xE} \in [-0.9, 0.2]$, the following plate follows the leading plate compactly. when $F_{xE} < -0.9$, the following plate will overtake the leading one; when $F_{xE} \geq 0.3$, the

compact mode will be broken, the two plates will form a regular mode ($F_{xE} = 0.3$) or the following plate will be dropped by the leading plate ($F_{xE} \geq 0.4$). For the regular configuration, the stable zone is $F_{xE} \in [-0.4, 0.3]$; when $F_{xE} < -0.4$, the following plate will form a compact configuration with the leading plate ($F_{xE} \geq -0.9$) or overtake the leader ($F_{xE} \leq -1.0$). A similar phenomenon was found in case 2, which will not be shown here. In the following discussion, this paper will focus on the emergent regular configuration.

Next, the stability of orderly configurations of two flapping flexible plates, with different types of external horizontal force exerting on the following plate, is studied. Table I lists four different functional forms of F_{xE} . For force type B, F_{B1} is the mean value of periodic external force, F_{B2} is the magnitude of the change of F_{xE} (if $F_{B2} = 0$, form B degenerates to form A). For type C and D, $2F_C$ and $2F_D$ are the maximal (or minimal) instantaneous value of F_{xE} , T_C/T and $2T_D/T$ are the ratio of the interval that F_{xE} is not zero to the total flapping period, $F_C \times T_C/T$ and $2F_D \times T_D/T$ are the mean value of F_{xE} , respectively. As is shown in Fig. 3(a), for case 1, whether or not the two plates can form a stable configuration depends only on F_{B1} . The stable state is independent of F_{B2} . When the mean value of $F_{xE}(t)$ satisfies $F_{B1} \geq 0.4$ (or ≤ -0.5), the following plate is subjected to a strong external resistance (or thrust), the gap spacing between the two plates will

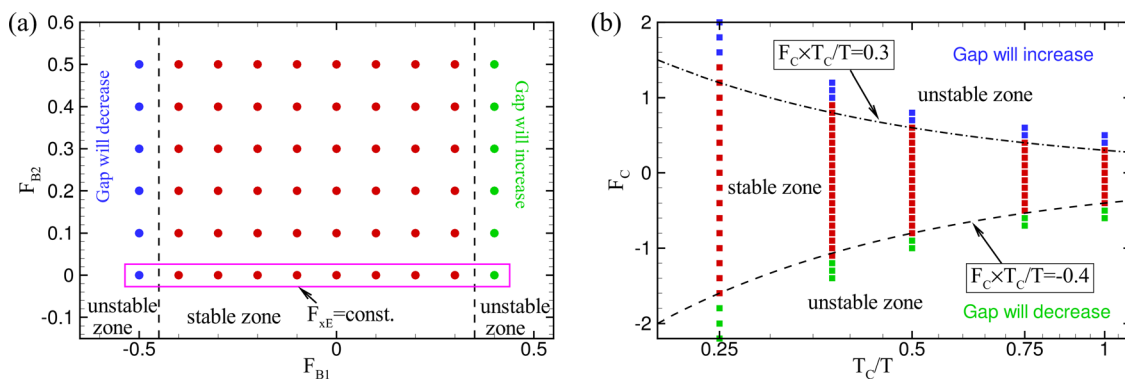


FIG. 3. Parameter space for two independently flapping plates of case 1. The force types of external horizontal force $F_{xE}(t)$ include (a) type A and type B, (b) type C in Table I.

increase (or decrease). And the stable regular configuration cannot be formed. If F_{B1} is within the stable zone $[-0.4, 0.3]$, the stable configurations will be spontaneously formed by different flow-mediated interactions for different F_{B1} . Figure 3(b) also shows that the stable state depends only on the mean value of the external force, $F_C \times T_C/T$, which does not depend on the amplitude (F_C) or interval of action (T_C) of the force alone. The stable space basically satisfies $F_C \times T_C/T \in [-0.4, 0.3]$. Our numerical simulations also confirm that the stable space of force type D in case 1 also satisfies $2F_D \times T_D/T \in [-0.4, 0.3]$ (figure is not shown). A similar phenomenon is found in case 2, where the corresponding stable space basically satisfies $\bar{F}_{xE} \in [-0.3, 0.4]$, and figures are not shown here. It is seen that the state of orderly configuration does not depend on the functional form of the external horizontal force, it just depends on the mean value of the force \bar{F}_{xE} .

The above results indicate that the two-plate system has certain ability to counteract the limited horizontal force intervention and maintain the orderly configuration. In other words, even if there is an external force intervention on the following plate, the following plate can harvest additional hydrodynamic force—through some specific vortex-follower interactions—to balance it. This further confirms Lighthill’s conjecture that the orderly configuration emerges passively from the hydrodynamic interactions.

For stable configurations, different equilibrium positions correspond to different vortex-plate interactions. For detailed analysis, the cases with a constant external horizontal force $F_{xE} = F_A$ on the following plate are considered first. Figure 4 shows the propulsive performance as functions of F_A for stable configurations. It is known that the wake of the leading plate is approximately composed of spatial periodic vortical structures, so there are multiple discrete positions with identical propulsive performance for each set of parameters, depending on the initial positions and phase difference of the leading and following plates.¹⁴ Here we denote $G^{eq,0}$ as the equilibrium gap spacing for $F_A = 0$, which is approximately integer multiples of wavelength λ . Figure 4(a) shows that applying an external horizontal force on the following plate hardly changes the propulsion speed U of the two plates. With the increase in the active external thrust, the equilibrium gap spacing between the plate plates decreases gradually, and vice versa.

The input work W and propulsion efficiency η of the following plate are shown in Fig. 4(b). It is noted that the oscillation of the leading edge of the plates and the work done by F_{xE} on the following plate are the energy inputs of the system. The input work is necessary to maintain the self-propulsion of the plates because the plates have to transfer energy to the fluid by interacting with it. It can be calculated through the time integral of power P_{fluid} produced by the plate during one flapping period, i.e.,

$$W = \int_{t_0}^{t_0+T} P_{fluid} dt = \int_{t_0}^{t_0+T} \left(\int_0^L \mathbf{F}_r(s, t) \cdot \frac{\partial \mathbf{X}}{\partial t}(s, t) ds \right) dt,$$

where F_r represents the force on the surrounding fluid from the plates. To quantify the propulsive efficiency of the plate, the ratio of the kinetic energy of the plate and the input power has been employed,⁵¹ i.e., $\eta = \frac{1}{2}MU^2/W$. It is seen from Fig. 4(b) that, the bigger the external horizontal force F_A , the greater the input work W , the smaller the propulsive efficiency. The input work of the leading plate is not affected by the external horizontal force F_{xE} on the following plate (figure is not shown). It means that by exerting an active thrust on the following plate, the energy consumption of the system can be reduced while maintaining a stable configuration.

Figures 5(a) and 5(b) show the following plate’s leading edge trajectories in the vortex street shed by the leading plate for case 1 and case 2, respectively. All stable trajectories are in the envelope of the blue line and the red line. For case 1, the stable trajectories vary between vortex locking¹⁴ and “slaloming between vortices,”¹⁰ depending on the active horizontal force F_{xE} ; and for case 2, the stable trajectories are closer to “vortex locking.” The stable trajectories of case 2 are much tighter than that of case 1.

To understand the influence of specific force type on propulsive performance, we first analyze case 1 with force type C. Figure 6 shows the propulsive performances as functions of F_C . T_C/T is the duty cycle. It is seen that for a stable configuration with fixed T_C/T , the greater the amplitude (F_C) of F_{xB} , the greater the gap spacing G^{eq} and the input power W . Generally speaking, the propulsion velocity decreases with the increase in F_C , but its change is very small (about 1.5%). For different T_C/T , the tendencies of propulsive performance varying with F_C are similar. The case with $T_C/T = 0.5$ is chosen to analyze the contributions of active horizontal force F_{xE} and the constraint

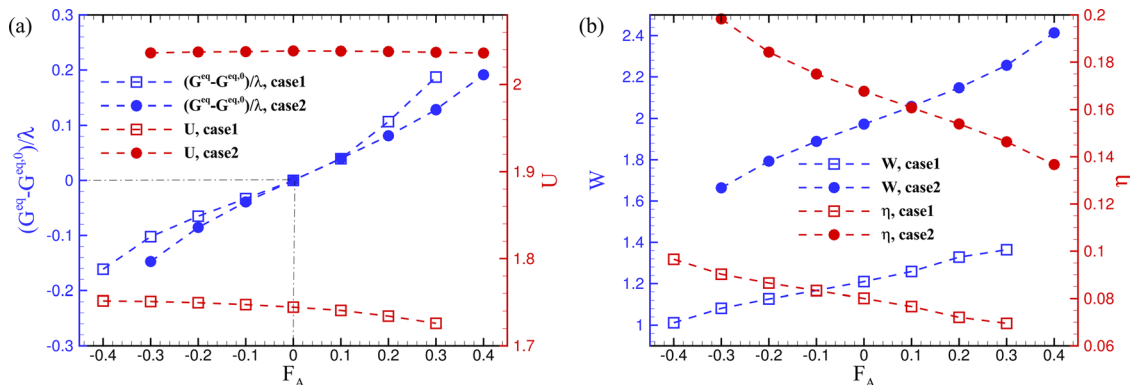


FIG. 4. (a) Gap spacing G^{eq} and propulsion velocity U , (b) input work W and propulsive efficiency η of the following plate as functions of mean value of external force $F_{xE} = F_A$ for case 1 and case 2.

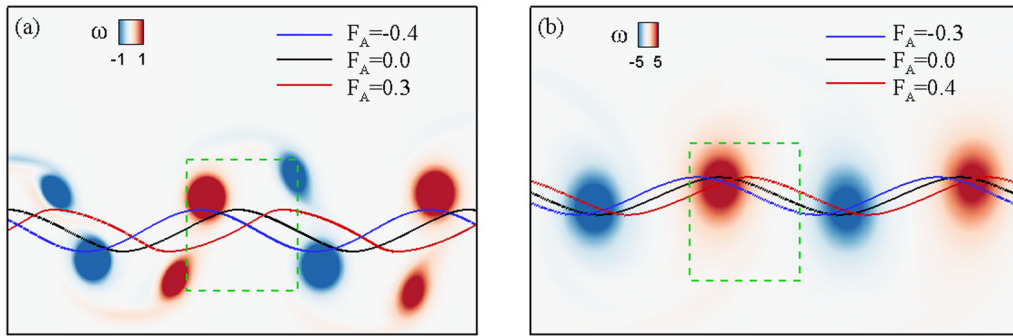


FIG. 5. Superimposition of the following plate's leading-edge trajectory for (a) case 1 and (b) case 2 on vortex street generated by one plate in isolated swimming.

vertical flapping motion to the input work, as shown in Fig. 6(d). It is seen that, when an external thrust is applied on the following plate, the input work contributed by flapping motion and the total input work will decrease. But if an external drag is applied on the following plate which causes negative work, there needs more input work done by the flapping motion to maintain the stable configuration.

As can be seen from Fig. 3 and its corresponding analysis, the key parameter affecting the stability of orderly configurations is the mean value $\bar{F}_{x\bar{E}}$ rather than its specific force function. To extract the key parameter that affects the propulsive performance, the mean value $\bar{F}_{x\bar{E}}$ is preferred. Figure 7 shows the propulsion performances as functions of $\bar{F}_{x\bar{E}}$ for force type C and three other types of force. For force type C,

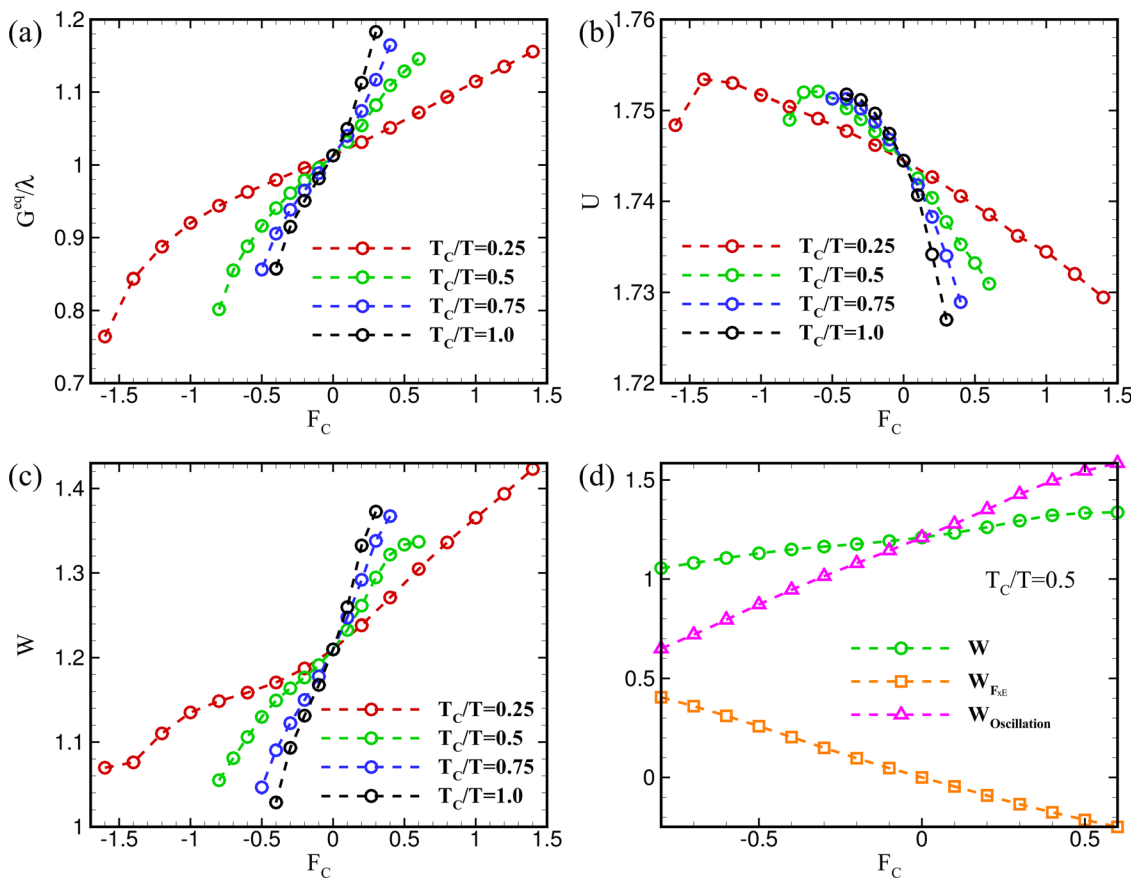


FIG. 6. (a) Equilibrium gap spacing G^{eq} , (b) propulsion velocity U , (c) input work W of the following plate as functions of F_c with external force of type C. (d) For $T_c/T = 0.5$, the total input work W , the work done by oscillation motion $W_{Oscillation}$, and the work done by $F_{x\bar{E}}$ as functions of F_c .

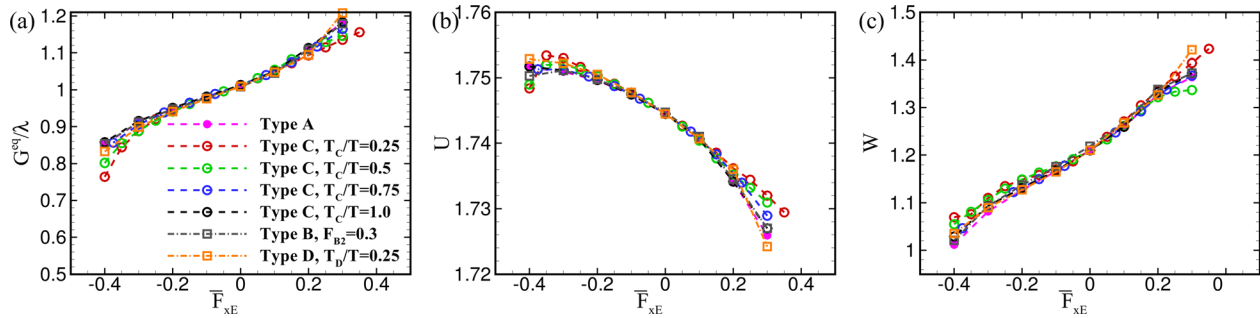


FIG. 7. (a) Equilibrium gap spacing G^{eq} , (b) propulsion velocity U , (c) input work W as functions of \bar{F}_{xE} with different types of external force.

$\bar{F}_{xE} = F_C \times T_C/T$. Compared with Fig. 6, the propulsive performances of different cases are almost normalized to the same curve with the change of the mean value \bar{F}_{xE} . It means that the key parameter affecting the propulsive performance is also the mean value rather than the functional form of specific force.

To further support the above conclusion, we analyzed the influence of different force forms of the same mean external horizontal force ($\bar{F}_{xE} = -0.2$) on the propulsive performance, and the results are shown in Fig. 8. Figures 8(a)–8(d) show four different forms of $F_{xE}(t)$

varying with time in one period, where $v (= \dot{y}_2)$ represents the vertical flapping velocity of the following plate. The four kinds of force are (a) force type B with $F_{B1} = -0.2$, and F_{B2} varying from 0.0 to 0.5; (b) force type C with $F_C = -0.4$, $T_C/T = 0.5$, $\Delta t/T$ varying from 0.0 to 1.0; (c) force type C with $\Delta t/T = 0.0$, T_C/T varying from 0.25 to 1.0; (d) force type D with $F_D = -0.4$, $T_D = 0.25$, $\Delta t/T$ varying from 0.0 to 1.0. Δt represents the phase difference between force F_{xE} and the flapping motion. For all four kinds, the variations of gap spacing G^{eq} , propulsion velocity U and input work W are within 1.5%, 0.2%, and

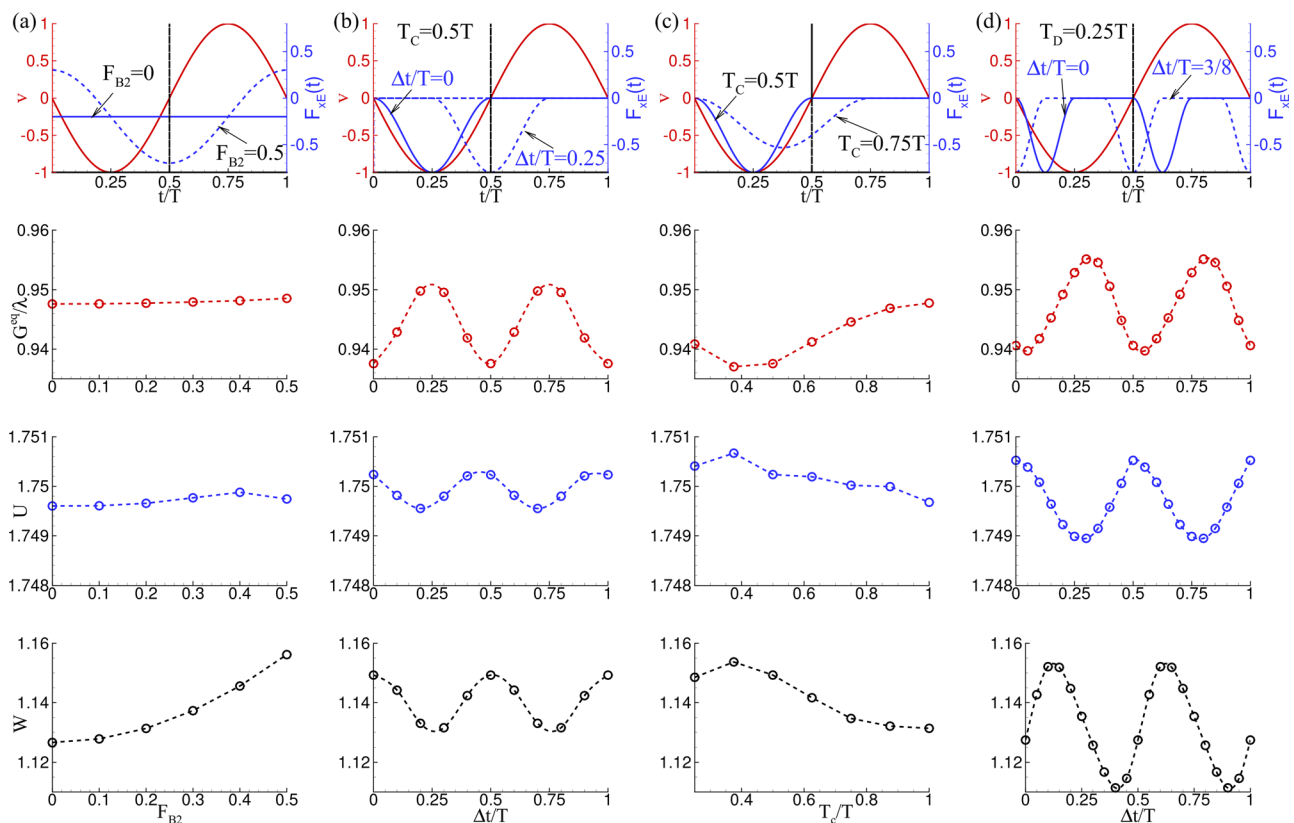


FIG. 8. Propulsive performance for identical mean value ($\bar{F}_{xE} = -0.2$) of external force with different function forms: Gap spacing G^{eq} , propulsion velocity U , input work W of the following plate for (a) force type B with different force amplitude F_{B2} , (b) force type C with $T_C = 0.5T$, Δt varying from 0 to T , (c) force type D with $\Delta t = 0$, T_C varying from 0.25 to 1.0, (d) force type D with $T_D = 0.25T$, Δt varying from 0 to T .

0.4%, respectively. It indicates that the propulsive performance is very little affected by the specific form of F_{xE} under the condition of fixed mean value \bar{F}_{xE} .

B. Simplified model for the follower-wake interaction

To explain the above findings, a simplified model is formulated to relate the external horizontal loading to the interaction of the following plate with the wake of the leading plate. See Appendix C for the detailed derivation. The model assumes that the thrust on each plate depends on the square of the plate’s vertical velocity relative to the ambient fluid, and the drag scales with the square of that plate’s propulsion velocity relative to the ambient fluid.^{32,56,57} In addition, an external horizontal force $F_{xE}(t)$ is exerted on the following plate. The motion of the leading plate can be regarded as an isolate plate swimming in stationary fluid. Its vertical and horizontal velocities relative to the ambient fluid are its own flapping velocity and propulsion velocity. For a stable configuration, the thrust and drag are proportional to $j_1^2 \propto (Af)^2$ and U^2 , respectively.

For the following plate, its relative velocity is its velocity minus the leading plate’s wake velocity at the same horizontal position. The horizontal velocity of the wake can be negligible. For a stable configuration, the drag is also proportional to U^2 . The wake’s vertical velocity at $x = x_2$ is assumed identical to that of the leading plate swimming through the same position. Then for a stable configuration of in-phase flapping, the hydrodynamic thrust on the following plate is proportional to $(\dot{y}_2 - v(x_2))^2 \propto U_{ref}^2 [1 - \cos(2\pi f \Delta t)]$. Here, $\Delta t = |x_1 - x_2|/U = (G^{eq} + L)/U$. Finally, in the time-average sense of Newton’s second law, the external horizontal force and gap spacing between two plates satisfy the following nondimensional relation:

$$\bar{F}_{xE} = \frac{c_t}{2} - c_t \cos\left(2\pi \frac{G^{eq} + 1}{\lambda}\right), \tag{5}$$

where the first term on the right is contributed by the vertical velocity $v(x_2)$ induced by the vortex street, which depends entirely on the flapping parameters of the leading plate. The second term on the right of Eq. (5) is contributed by the coupling between the vortex street and the flapping following plate, which depends on the kinematic parameters of both plates and external active intervention. It is seen from expression Eq. (5) that, for stable regular configuration, the

equilibrium gap spacing depends on the mean value of the external horizontal force rather than the force’s specific form.

For case 1 and case 2, the Strouhal number, $St = 2Af/U$, is about 0.182 and 0.156, respectively. Hence, in the current work, the thrust coefficient c_t are selected as 0.8 and 0.55,^{56,57} respectively. By substituting the thrust coefficients into expression Eq. (5), we predict the relationship between \bar{F}_{xE} and G^{eq} for case 1 and case 2, as shown in Fig. 9. The numerical data on external horizontal force and equilibrium gap spacing for different types of forces are compared with the theoretical prediction. It is seen that the data points in the numerical simulation basically fall on the PSS of the theoretical curve, which agrees with the stability analysis of Fig. 15 in Appendix C. It is noted that the numerical data points do not occupy the whole PSS of the curve due to the simplification of the model. The model ignores some important factors such as the complex interactions of the following plates with the vortex street, unsteady flow separation on the plates, and the dissipation of vortices, etc.

C. Force and power linked to local vortical structures

The previous analysis indicates that, different external horizontal force leads to different follower’s trajectory in the reversed Kármán vortex street shed by the leader, as shown in Fig. 5. Different trajectories mean different interactions between the follower and the vortex street, which results in different flow field characteristics, momentum and energy transferred to the fluid. In this section, we first show the characteristics of the flow field under different external horizontal force, then link the momentum and energy transfer to local vortical structures.

Figure 10 shows the instantaneous vortical structures for different external active force ($F_{xE} = -0.4, 0.0, \text{ and } 0.3$) in case 1. At the instantaneous moment, $t = nT$, the y-coordinate of the leading edge of the plate is A (flapping amplitude), and the flapping direction begins to change. From Fig. 10(a), it is seen that the following plate passes through the vortex core of the stronger positive vortex in a pair of vortices. By comparing Figs. 10(a)–10(c), it is seen that consistent with Fig. 5(a), the trajectory gradually moves backward with the increase in external force F_{xE} . For $F_{xE} = -0.4$, the clockwise (or counterclockwise) vorticity generated on the following plate will merge with the vortices of the same direction shed by the leading plate, and eventually

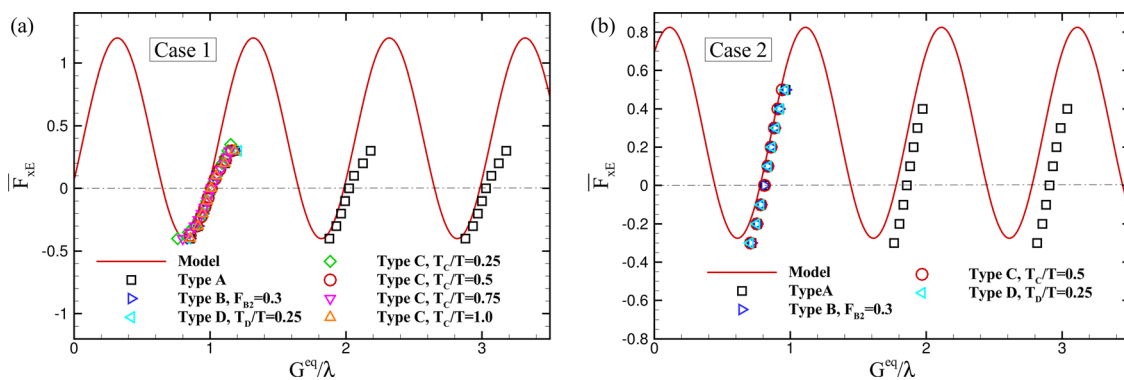


FIG. 9. Theoretical prediction and numerical simulation of the relation between external horizontal force on the following plate and the gap spacing G^{eq} for (a) case 1 and (b) case 2.

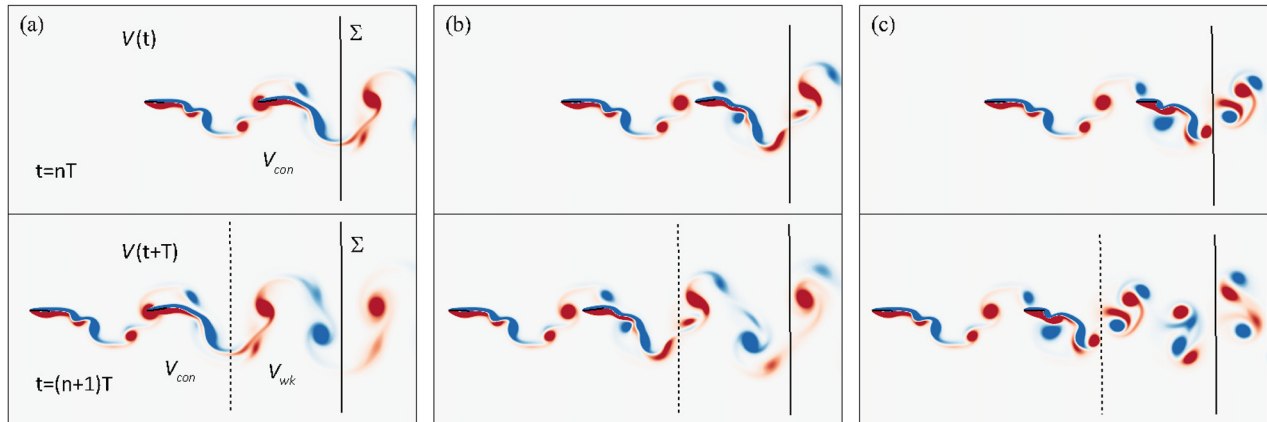


FIG. 10. The instantaneous vorticity fields for case 1 with (a) $F_{xE} = -0.4$, (b) $F_{xE} = 0.0$, (c) $F_{xE} = 0.3$ at $t = nT$ and $t = (n + 1)T$, respectively.

form a larger vortex in the wake of the following plate. For $F_{xE} = 0.3$, the following plate slaloms between the vortex cores, the clockwise (counterclockwise) vorticity generated on the following plate and the counterclockwise (clockwise) vortices shed by the leading plate will wind around each other. When the parameter F_{xE} gradually increases from -0.4 to 0.3 , the vorticity separation on the following plate is gradually strengthened, and the wake gradually transitions from the state of “codirectional vortices merging” to the state of “opposite-directional vortices winding.”

Different flow field structures indicate that the plates transfer different momentum and energy to the surrounding flow field (see Fig. 16 in Appendix D). The mean values of hydrodynamic force and input work are key parameters. Hence, the relationship between the external horizontal force and the change of the momentum and energy of the flow field in a period is highlighted in the following analysis. As shown in Fig. 10, after a period of self-propulsion, a pair of additional vortices appear in the downstream of the following plate, of which the domain is denoted by V_{wk} . Figure 17 in Appendix D shows statistics of the strength of such a pair of vortices in the wake of the following plate. It is seen that with the increase in F_{xE} , the strength of the vortex pair in the wake of the following plate gradually increases.

Next, we aim to quantitatively relate the characteristics of the flow field with the propulsive performance under different vortex-plate interactions. Considering that the propulsive performance of an object is mainly related to the flow structures surrounding the object,^{44,58,59} for two-dimensional incompressible flow, the hydrodynamic force on the plates and the power that is transferred from the plates to the fluid are expressed as

$$\mathbf{F}(t) = -\frac{d\mathbf{I}}{dt} + \mathbf{F}_l + \mathbf{F}_B + \mathbf{F}_\Sigma, \quad (6)$$

$$P_{fluid}(t) = \frac{dK}{dt} + \Phi + P_B + P_\Sigma, \quad (7)$$

where

$$\begin{aligned} \mathbf{I} &= \int_{V(t)} \mathbf{x} \times \rho \boldsymbol{\omega} dV, & \mathbf{F}_l &= -\int_{V(t)} \rho \boldsymbol{\omega} \times \mathbf{u} dV, \\ \mathbf{F}_B &= \int_{\partial B} [\mathbf{x} \times (\mathbf{n} \times \rho \mathbf{a}) + \mathbf{x} \times \rho \mathbf{u}(\boldsymbol{\omega} \cdot \mathbf{n})] dS, \end{aligned} \quad (8)$$

$$K = \int_V \rho \frac{|\mathbf{u}|^2}{2} dV, \quad \Phi = \int_V \mu \boldsymbol{\omega}^2 dV, \quad P_B = -\frac{d}{dt} \int_{V_B} \rho \frac{|\mathbf{u}|^2}{2} dV. \quad (9)$$

Here $V(t)$ denotes the material analysis domain, and has an external boundary Σ ; \mathbf{I} and K represent the vortical impulse and kinetic energy, with ρ being the fluid density, \mathbf{x} being the position vector; \mathbf{F}_l is the vortex force;⁴³ Φ denotes the dissipation caused by entropy, which is directly related to the reduction of kinetic energy. \mathbf{n} is the normal vector. $\mathbf{a} = d\mathbf{u}/dt$ is the acceleration. ∂B and V_B are the boundary and domain of the body, respectively. Since the plates in our simulation has no thickness, \mathbf{F}_B and P_B are zero. Finally, \mathbf{F}_Σ and P_Σ are surface integrals on Σ , i.e.,

$$\begin{aligned} \mathbf{F}_\Sigma &= \int_\Sigma \mathbf{x} \times \rho \mathbf{u}(\boldsymbol{\omega} \cdot \mathbf{n}) dS + \int_\Sigma \mu [\mathbf{x} \times (\mathbf{n} \cdot \nabla \boldsymbol{\omega}) + \boldsymbol{\tau}] dS, \\ P_\Sigma &= \int_\Sigma (\rho \mathbf{n} - \boldsymbol{\tau}) \cdot \mathbf{u} dS, \end{aligned}$$

where $\boldsymbol{\tau} = \mu \boldsymbol{\omega} \times \mathbf{n}$ is the viscous force.

The expressions Eqs. (6) and (7) are used to analyze the results of flapping plates. For clarity, here we use case with $F_{xE} = -0.4$ as an example to perform detailed analysis. $V(t)$ is chosen as a material analysis domain as shown in Fig. 10, letting Σ (denoted by the black solid line) cutting as less vorticity as possible. Theoretically, when the outer boundary Σ of the material domain satisfies: $\boldsymbol{\omega} = \mathbf{0}$ at and near Σ , \mathbf{F}_Σ can be ignored.⁴⁴ At $t = nT$, the material domain $V(t) (= V_{con})$ consists of the vorticity on the left side of Σ . After a period of self-propulsion, there is an additional pair of vortices appear in the material domain, i.e., $V(t + T) = V_{con} + V_{wk}$.

Figure 11 shows the time-dependent horizontal hydrodynamic force F_x and power transferred to fluid P_{fluid} , where F_x is the stream-wise component of \mathbf{F} . It is seen that F_x and P_{fluid} calculated by Eqs. (6) and (7) agree well with the standard results F_{STD} and P_{STD} . It is noted that F_{STD} is calculated by the sum of $\int_0^L F_s(s, t) ds$ on the two plates, and P_{STD} is calculated by the sum of $\int_0^L \mathbf{F}_r(s, t) \cdot \frac{\partial \mathbf{x}(s, t)}{\partial t} ds$ on the two plates. From Fig. 11(a), it is seen that the horizontal force contributed by \mathbf{F}_Σ can be ignored because the outer boundary Σ hardly cuts

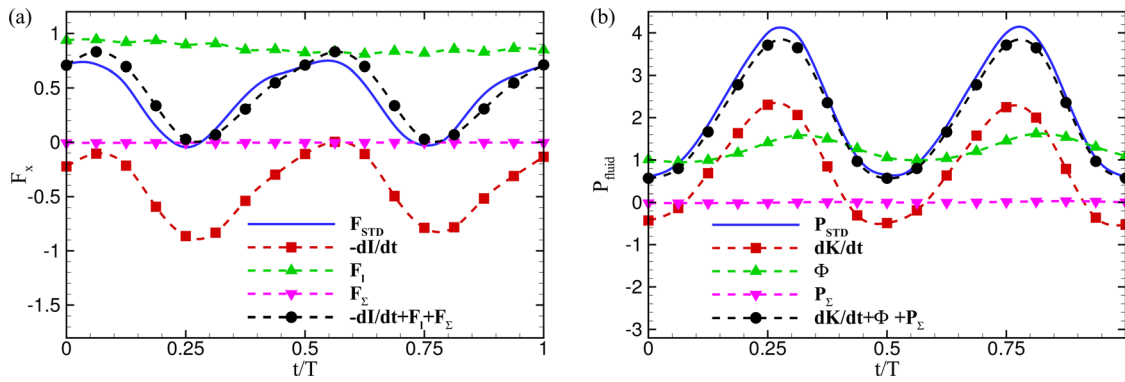


FIG. 11. (a) The horizontal hydrodynamic force F_x and (b) power transferred to the fluid P_{fluid} as functions of time for case 1 with $F_{xE} = -0.4$.

vortices. Results also show that the force contributed by the vortex force is positive and hardly changes with time. It is a natural result, since the vortex force integral in the whole space is zero, i.e., $\int_{V_\infty} \rho \boldsymbol{\omega} \times \mathbf{u} dV = 0$,⁴³ the variation of F_l is identical with $\int_{V_\infty} \rho \boldsymbol{\omega} \times \mathbf{u} dV$. The latter changes slowly over time because its variation is caused by the weak induction and dissipation of vortices in the wake. Previous works⁶⁰ indicate that, for two-dimensional incompressible steady flow with high Reynolds number, the vortex force contributes to the total drag of the body. According to the analysis of Sec. III B, the drag depends on the square of the horizontal velocity relative to the ambient fluid. Since the variation of such horizontal velocity is very small compared with the time-average propulsion velocity U , the variation of the vortex force should also be small. This is another interpretation for the characteristics of the vortex force. Figure 11(a) also shows that the hydrodynamic thrust is mainly contributed by the impulse force. As discussed in Sec. III B, the thrust depends on the square of the vertical flapping velocity relative to the ambient, which changes significantly over time. Hence, the time dependence of instantaneous hydrodynamic force $F_x(t)$ is mainly represented by the impulse force term. Figure 11(b) shows that P_Σ can be ignored, since $\mathbf{u} \cdot \mathbf{n}$ on Σ can be ignored when the normal direction of the wake section of the outer boundary Σ satisfies: $\mathbf{n} = \mathbf{e}_x$, as shown in Fig. 10. The time dependence of the power transferred to the fluid is mainly contributed by the kinetic energy term, which is positive for most of the time of a period. The power transferred to dissipation is positive all the time.

As shown in Fig. 10, the flow field at a certain moment has one more pair of vortices than that of one period ago. To understand the relationship between such additional vortex pair and the transfer of the momentum and power from the plates to the fluid, by choosing the special domain as shown in Fig. 10, we obtain the following expressions by integrating Eqs. (6) and (7) over a period of time,

$$\mathbf{I}_{wk} = \int_t^{t+T} \mathbf{F}_{xE}(t') dt' - \left(- \int_t^{t+T} \mathbf{F}_l(t') dt' \right), \quad (10)$$

$$K_{wk} = \int_t^{t+T} P(t') dt' - \int_t^{t+T} \Phi(t') dt', \quad (11)$$

where

$$\mathbf{I}_{wk} = \int_{V_{wk}} \mathbf{x} \times \rho \boldsymbol{\omega} dV, \quad K_{wk} = \int_{V_{wk}} \rho \frac{|\mathbf{u}|^2}{2} dV.$$

Here \mathbf{I}_{wk} and K_{wk} are the total impulse and kinetic energy of the nearest pair of vortices downstream of the following plate respectively. The first term on the right of Eq. (10) is the total momentum transferred from the plate to the fluid in one period, which is contributed entirely by the external horizontal force. The second term on the right of Eq. (10) is the momentum to overcome the drag contributed by the vortex force. The two terms on the right of Eq. (11) are the total energy transferred to the fluid and the energy for dissipation respectively. Figure 12(a) shows that the increase in horizontal momentum in a period, $\mathbf{I}_{wk} \cdot \mathbf{e}_x$, is positive and hardly varies with the external horizontal force. The momentum to overcome the drag contributed by the vortex force is negative and increases with F_{xE} . The sum of the above two terms agrees well with the total momentum transferred to the fluid. Figure 12(b) shows that the power transferred to the kinetic energy of the fluid decreases as F_{xE} increases, while the dissipation of the fluid increases as F_{xE} increase. This result is natural, since as shown in Fig. 10, when F_{xE} increases, the vortices shed by the following plate will increase.

IV. CONCLUSIONS

In summary, the effect of an external horizontal force on the self-organization of two self-propelled flapping plates in a tandem configuration is studied in this paper. In the process of the two self-propelled flapping plates moving forward, external horizontal forces of different functional forms are applied to the leading edge of the following plate. Results show that even with limited external active control, the orderly configurations can still emerge passively from the hydrodynamic interactions. This is further support to Lighthill's conjecture. Of course, if the external force intervenes too strongly, the orderly configuration will be broken. Moreover, we find that the stability and propulsive performance of the orderly configurations are mainly affected by the mean value of the external horizontal force rather than its specific functional form. To our knowledge, it is the first time that verifies Lighthill's conjecture in the condition of external active control and find that the group cohesion is affected by the mean value of the external horizontal force rather than its functional form.

The reversed Kármán vortex street shed by the leading plate has a certain robustness to resist the active intervention and maintain

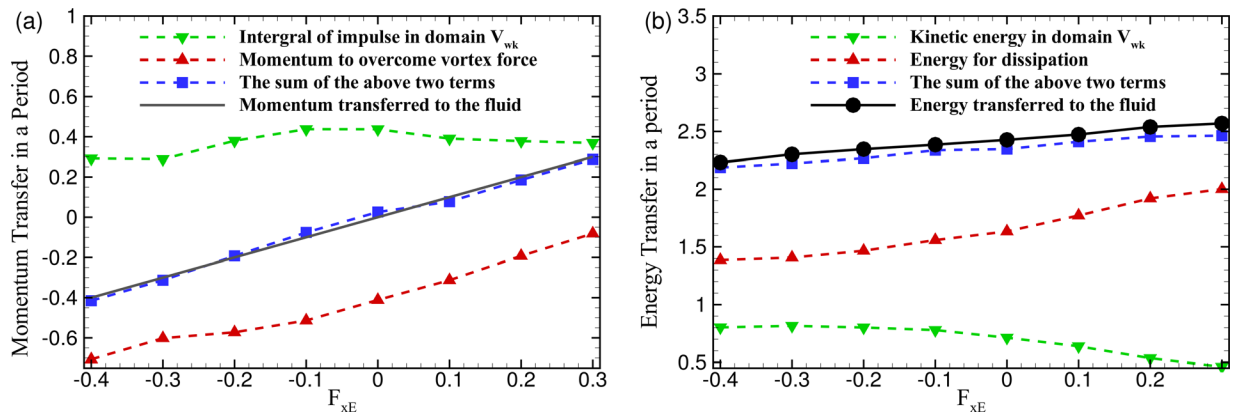


FIG. 12. The transfer of (a) momentum and (b) energy in a period calculated by Eqs. (10) and (11).

orderly configurations of the collective motion. When the external horizontal force is within a stable range, the plates propel in an orderly configuration. Once the mean value (\bar{F}_{xE}) of the external horizontal force is out of the stable range, the follower will break free of the vortex street, either colliding with (or passing over) the leader or being dropped by it. For stable configurations, the bigger the mean value of external horizontal force, the bigger the equilibrium gap spacing between the two plates, and the more energy is transferred to the fluid. With the increase in \bar{F}_{xE} , the trajectory of the follower in the vortex street gradually transfers from the “vortex locking” behavior to the “slaloming between vortices” behavior. A simplified model is proposed which relates the mean value of the active horizontal force to the gap spacing of the two plates, which shows good agreement with the numerical results.

Finally, the transfer of momentum and energy of the two-plate system is investigated in terms of local vortical structures. The horizontal component of the momentum transferred to the fluid is entirely provided by the active horizontal force F_{xE} . Results show that, for stable configuration, with the increase in \bar{F}_{xE} , more vorticity is generated on the following plate. The horizontal component of the impulse of a pair of vortices in the wake of the following plate is almost not affected by the active loading, while the momentum against the drag contributed by the vortex force increases linearly with \bar{F}_{xE} . The kinematic energy of a pair of vortices downstream of the following plate decreases with the increase in external horizontal loading. However, vortex dissipation of the flow field increases and the total energy output eventually increases with the increase in \bar{F}_{xE} .

Although the geometric shape and actuation are simplified, this study is essential for understanding the underlying mechanism of collective behavior in fish schools. It also inspires the development of swarm intelligence. For example, with limited active control, the follower can explore the most energy-effective position in a stable configuration.

ACKNOWLEDGMENTS

L.K. and W.C. acknowledge the “Construction of a Leading Innovation Team” project by the Hangzhou Municipal government and the Startup funding of New-joined PI of Westlake University (Grant No. 041030150118). X.-Y.L. and H.H. acknowledge the

support of the National Natural Science Foundation of China (Grant Nos. 11872064 and 11621202). Z.-R.P. acknowledges the support of the National Natural Science Foundation of China (Grant No. 11902120).

AUTHOR DECLARATIONS

Conflict of Interest

The authors have no conflicts to disclose.

APPENDIX A: THE NUMERICAL METHOD DETAILS

In the present work, the kinetics of the fluid is governed by the discrete lattice Boltzmann equation (LBE) of a single relaxation time model,^{46,61,62} and the multi-block lattice Boltzmann technique⁶³ has been incorporated. The LBE with the Bhatnagar–Gross–Krook (BGK) model⁶⁴ is

$$f_i(\mathbf{x} + \mathbf{e}_i \Delta t, t + \Delta t) - f_i(\mathbf{x}, t) = -\frac{1}{\tau} [f_i(\mathbf{x}, t) - f_i^{eq}(\mathbf{x}, t)] + \Delta t F_i, \quad i = 0, \dots, 8, \quad (A1)$$

where f_i is the i th particle distribution function with discrete speed \mathbf{e}_i at position \mathbf{x} and time t . Δx and Δt are the grid spacing and time step, respectively. $\tau = (\nu/c_s^2 \Delta t + 0.5)$ is the nondimensional relaxation time associated with kinematic viscosity ν , where $c_s = (\Delta x/\Delta t)/\sqrt{3}$ is the lattice sound speed. The equilibrium distribution function f_i^{eq} and the forcing term F_i are defined as^{61,65}

$$f_i^{eq} = \omega_i \rho \left[1 + \frac{\mathbf{e}_i \cdot \mathbf{u}}{c_s^2} + \frac{\mathbf{u} \mathbf{u} : (\mathbf{e}_i \mathbf{e}_i - c_s^2 \mathbf{I})}{2c_s^4} \right], \quad i = 0, \dots, 8, \quad (A2)$$

$$F_i = \left(1 - \frac{1}{2\tau} \right) \omega_i \left[\frac{\mathbf{e}_i - \mathbf{u}}{c_s^2} + \frac{\mathbf{e}_i \cdot \mathbf{u}}{c_s^4} \mathbf{e}_i \right] \cdot \mathbf{f}, \quad i = 0, \dots, 8, \quad (A3)$$

where ω_i is the weighting factor depending on the lattice model ($\omega_0 = 4/9, \omega_1 = \omega_2 = \omega_3 = \omega_4 = 1/9, \omega_5 = \omega_6 = \omega_7 = \omega_8 = 1/36$). ρ, \mathbf{u} , and \mathbf{f} are the macroscopic fluid density, velocity, and body force, respectively, as defined in Eq. (2).

The mass density and velocity can be obtained by the distribution functions,

$$\rho = \sum_i f_i, \tag{A4}$$

$$\rho \mathbf{u} = \sum_i \mathbf{e}_i f_i + \frac{1}{2} \mathbf{f} \Delta t. \tag{A5}$$

Equation (4) for the plate is discretized by a finite element method. The motion of the plate is handled by the corotational scheme.⁴⁸ In this scheme, a local coordinate system is envisioned to move with each discrete element, and the element behaves linearly relative to the moving coordinate system. Consequently, the nonlinearity of the problem goes to the coordinate transformation.

In the IB method, the Lagrangian interaction force F_s [used in Eq. (4)] can be calculated by the feedback law,⁴⁹

$$F_s(s, t) = \alpha \int_0^t [V_f(s, t') - V_s(s, t')] dt' + \beta [V_f(s, t) - V_s(s, t)], \tag{A6}$$

where α and β are free parameters to enforce the no-slip condition, which are selected based on Hua *et al.*⁵¹ V_f is the fluid velocity at the position of the body, which is obtained by interpolation

$$V_f(s, t) = \int_{\Gamma} \mathbf{u}(\mathbf{x}, t) \delta(\mathbf{x} - \mathbf{X}(s, t)) d\mathbf{x}, \tag{A7}$$

where the plate boundary Γ is denoted by the Lagrangian coordinates $\mathbf{X}(s, t)$. The Eulerian body force \mathbf{f} [used in Eq. (2)] can be calculated as

$$\mathbf{f}(\mathbf{x}, t) = - \int_{\Gamma} F_s(s, t) \delta(\mathbf{x} - \mathbf{X}(s, t)) ds. \tag{A8}$$

In the present work, a four point regularized δ function⁴⁹ is used.

APPENDIX B: THE VALIDATION AND GRID INDEPENDENCE STUDY

To validate the numerical method used in the present study, the locomotion of two self-propelled plates swimming in tandem is simulated with parameters $A = 0.5$, $Re = 200$, $M = 0.2$, $K = 0.8$,

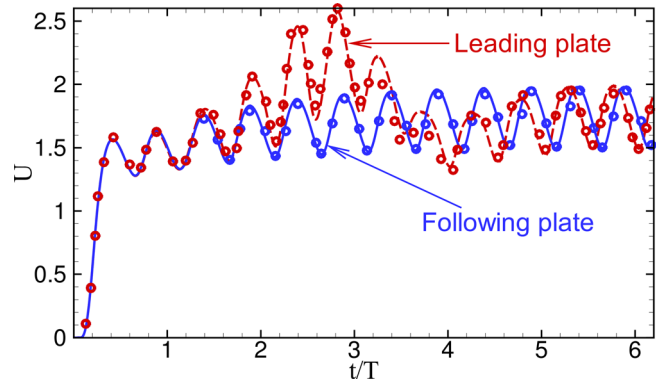


FIG. 13. Numerical validation. The time evolution of the propulsion velocity U of the plates. Lines and symbols represent the present results and those in Ref. 14. In the case, the key parameters are: $Re = 200$, $A = 0.5$, $M = 0.2$, $K = 0.8$, $S = 1000$, $F_{xE} = 0$, and the initial gap spacing $G_0 = 7.0$.

$S = 1000$, and $F_{xE} = 0$. The parameters in the simulation are identical to those in Zhu *et al.*¹⁴ Figure 13 shows the time history of the propulsion velocities of both plates. It is seen that the propulsion velocities of both plates are consistent with those from Zhu *et al.*¹⁴

To study the grid independence and time step independence, the locomotion of two self-propelled plates in a tandem configuration with an external horizontal loading F_{xE} on the following plate is simulated. The parameters are $A = 0.5$, $Re = 200$, $M = 0.2$, $K = 0.8$, $S = 1000$, and F_{xE} is chosen as type C with $F_C = -0.5$ and $T_C = 0.5T$. The propulsion velocity and horizontal force of the following plate in simulations with different mesh size and time step size are shown in Fig. 14. It is seen that $\Delta x/L = 0.01$ and $\Delta t/T = 0.0001$ are sufficient to achieve accurate results.

APPENDIX C: SIMPLIFIED DYNAMICAL MODEL

Here we consider the swimming of the flapping plates, labeled $i = 1, 2$ for the leader and follower respectively. The plates swim along the negative x direction, and the flapping function satisfies

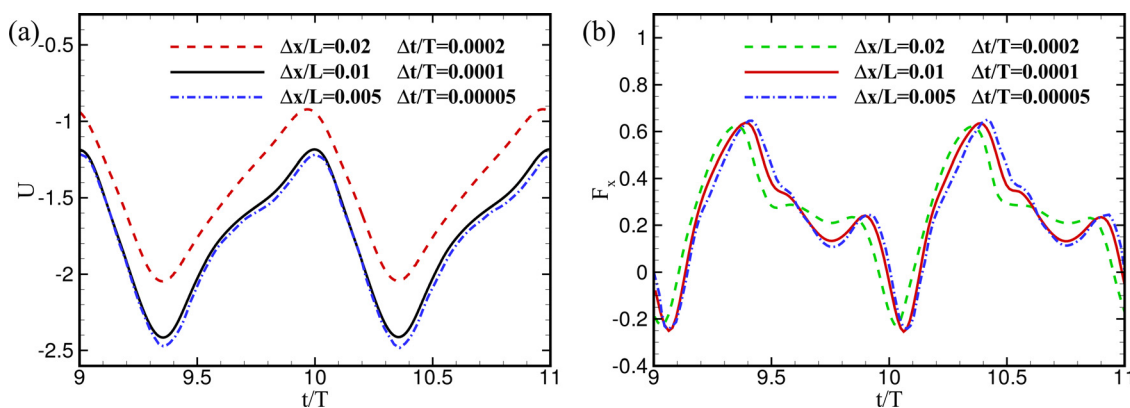


FIG. 14. The grid independence and time step independence studies for the case with $Re = 200$, $A = 0.5$, $M = 0.2$, $K = 0.8$, $S = 1000$. The external force is described by force type C in Table I with $F_C = -0.5$ and $T_C = 0.5T$. The time evolution of (a) the propulsion velocity U and (b) horizontal hydrodynamic force F_x of the following plate.

$$y_1(t) = y_2(t) = A \cos(2\pi ft). \quad (C1)$$

In addition, an external horizontal force $F_{xE}e_x$ is applied on the follower. According to Newton's second law, there is

$$m\ddot{x}_1 = -T_1 + D_1, \quad m\ddot{x}_2 = F_{xE} - T_2 + D_2, \quad (C2)$$

where m is the mass of the plate, T_i and D_i are the hydrodynamic thrust and drag on the i th plate. Previous works^{32,56,57} indicate that the thrust on each plate is proportional to the square of the plate's vertical velocity relative to the ambient fluid, and the drag depends on the square of that plate's propulsion velocity relative to the ambient fluid, i.e.,

$$T_i = \frac{1}{2} \rho L c_t (\dot{y}_i - v(x_i))^2, \quad D_i = \frac{1}{2} \rho L c_d (\dot{x}_i - u(x_i))^2, \quad (C3)$$

where c_t and c_d are (constant) thrust and drag coefficients, ρ is the fluid density, L is the length of the plate. It is noted that, according to classic Blasius theory, the drag coefficient $c_d (\sim Re^{-1/2})$ is given in terms of the Reynolds number. Hence, the drag force usually scales as $(\rho \mu L)^{1/2} U^{3/2}$.⁶⁶ In our simulation, the Reynolds number is constant, hence c_d is constant, and the drag depends on the square of swimming velocity relative to ambient fluid.

Since the leader always swims into still fluid, there is $u(x_1) = v(x_1) = 0$, then

$$m\ddot{x}_1 = \frac{1}{2} \rho L [-c_t \dot{y}_1^2 + c_d \dot{x}_1^2]. \quad (C4)$$

Integrating the above equation over one time period, the term on the left will disappear, since the leader can be assumed as an isolated, periodic swimmer. Then we can obtain

$$\overline{\dot{x}_1^2} = \frac{c_t}{c_d} \overline{\dot{y}_1^2}, \quad (C5)$$

where $\overline{\dot{x}_1^2} = \int_{t_0}^{t_0+T} \dot{x}_1^2 dt / T$. For stable configurations, the form of \dot{x}_1 should be a function like $U_1 + B_1(t)$, where U_1 is the propulsive velocity. Since usually $|B_1(t)| \ll |U_1|$, we can assume that $\overline{\dot{x}_1^2} = U_1^2$. By Eq. (C1), we can obtain $\overline{\dot{y}_1^2} = (2\pi Af)^2 / 2$. Finally, for the leading plate, there is

$$U_1 = 2\pi Af \sqrt{\frac{c_t}{2c_d}}. \quad (C6)$$

The following plate swims into the reversed Kármán vortex street shed by the leading plate. Its dynamical equation is

$$m\ddot{x}_2 = F_{xE} + \frac{1}{2} \rho L [-c_t (\dot{y}_2 - v(x_2))^2 + c_d (\dot{x}_2 - u(x_2))^2]. \quad (C7)$$

Usually horizontal velocity of the wake can be ignored, i.e., $u(x_2) = 0$. The vertical velocity of the wake in lab frame can be assumed equal to the leader's vertical flapping velocity as it swims by,³² i.e., $v(x_2) = \dot{y}_1(t - \Delta t)$, where $\Delta t = (G^{eq} + L) / U_1$ is determined by the gap spacing between two plates. By Eq. (C1), there is

$$\begin{aligned} (\dot{y}_2 - v(x_2))^2 &= (2\pi A t)^2 \left[\frac{1 - \cos(4\pi f t)}{2} + \frac{1 - \cos(4\pi f(t - \Delta t))}{2} \right] \\ &\quad - 2(2\pi A f)^2 \left[\frac{\cos(2\pi f \Delta t) - \cos(4\pi f t - 2\pi f \Delta t)}{2} \right]. \end{aligned} \quad (C8)$$

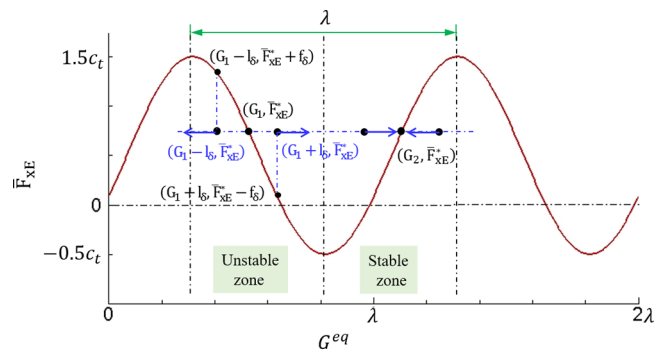


FIG. 15. Diagram of stability analysis of equilibrium gap spacing. $l_\delta > 0$, $f_\delta > 0$.

For the stable configuration of the collective locomotion, there is

$$\overline{m\ddot{x}_2} = 0, \quad \overline{\dot{x}_2^2} = \overline{\dot{x}_1^2}, \quad \overline{(\dot{y}_2 - v(x_2))^2} = (2\pi Af)^2 [1 - \cos(2\pi f \Delta t)].$$

Making time-average of Eq. (C7), we can obtain the following non-dimensional relation:

$$\overline{F_{xE}} = \frac{c_t}{2} - c_t \cos\left(2\pi \frac{G^{eq} + 1}{\lambda}\right). \quad (C9)$$

Figure 15 shows the relationship between the equilibrium gap spacing G^{eq} and the mean value $\overline{F_{xE}}$ of the external horizontal force, which is calculated by Eq. (5). It is seen that within the range of a wavelength λ , the same mean value of the external horizontal force ($\overline{F_{xE}^*}$ for example) corresponds to two equilibrium gap spacings (G_1 and G_2). $(G_1, \overline{F_{xE}^*})$ is on the negative slope side (NSS) of the curve. If the following plate is disturbed and deviates from this equilibrium position, for example the gap space between two plates becomes $(G_1 \mp l_\delta)$, then the following plate will obtain a hydrodynamic force $-(\overline{F_{xE}^*} \pm f_\delta)$. And the net horizontal force on the following plate will be $\mp f_\delta$, which pull the following plate closer to (or further away from) the leading plate, and hence away from the equilibrium position G_1 . This means that, for a given $\overline{F_{xE}^*}$, G_1 on NSS of the curve is an unstable equilibrium gap spacing, and a small perturbation will move it away from the equilibrium position. Using the same analysis, we can find that G_2 on the positive slope side (PSS) of the curve is a stable gap spacing. If the following plate is disturbed and deviates from this equilibrium position, the hydrodynamic force will push the following plate back to the equilibrium position G_2 .

APPENDIX D: SOME SUPPORTING INFORMATION FOR SEC. III C

Figure 16 shows the evolution of the force (F_x) on the plate and the power (P_{fluid}) transferred to the fluid under the intervention of different active loading. It is seen that, without an active loading on the following plate, the evolution of force and power transfer on the following plate is similar to that on the leading plate, except there is a phase shift. For a thrust type of active intervention ($F_{xE} = -0.4$ for example), the following plate obtains a hydrodynamic drag to balance the active intervention by vortex locking

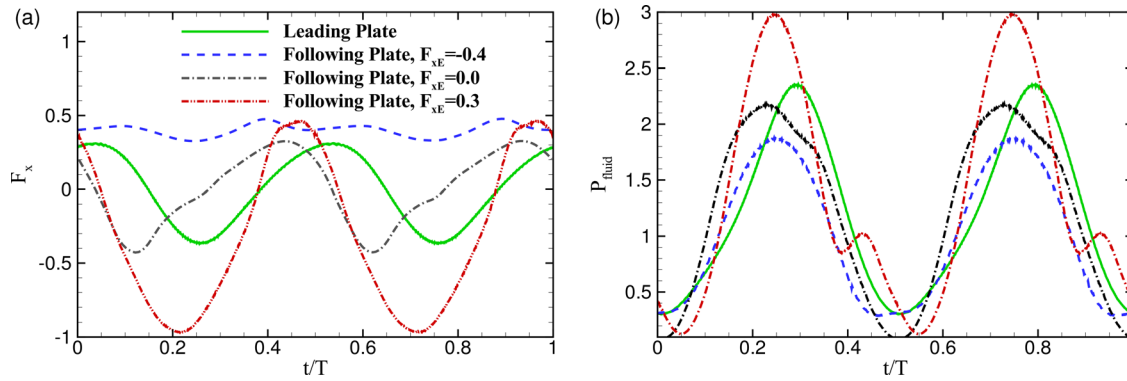


FIG. 16. The time evolution of (a) the horizontal component of the hydrodynamic force (F_x) on the plates and (b) power (P_{fluid}) transferred to the fluid for case 1 with a constant external horizontal force F_{xE} .

behavior,¹⁴ as shown in Figs. 5(a) and 10(a). There is less power transferred to the fluid. For a drag type of active intervention ($F_{xE} = 0.3$ for example), the following plate obtains more hydrodynamic thrust by slaloming between vortices behavior,¹⁰ as shown in Figs. 5(a) and 10(c), but there is more power transferred to the fluid.

Figure 10 shows that, after a period of self-propulsion, a pair of additional vortices appear in the downstream of the following plate, of which the domain is denoted by V_{wk} . Figure 17 shows statistics of the strength of such a pair of vortices in the wake of the following plate, which is calculated by $\int_{V_{wk}} |\omega|/2dV$. The strength of the newly generated vortices on the following plate is roughly estimated by subtracting the strength of a pair of vortices shed by the leading plate from $\int_{V_{wk}} |\omega|/2dV$. It is seen that with the increase in F_{xE} , the strength of the vortex pair in the wake of the following plate gradually increases. Especially when $F_{xE} > 0$, the increase is very significant. For 2D incompressible flow, the evolution of vorticity in the flow field satisfies $d\omega/dt = \nu \nabla^2 \omega$, which means that the evolution of vorticity is contributed only by the viscosity diffusion effect.

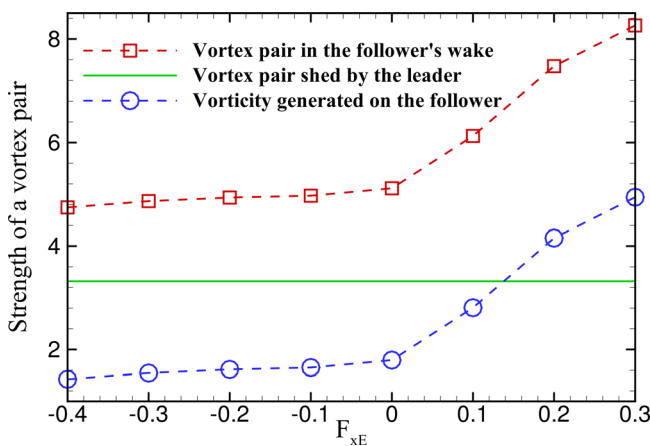


FIG. 17. The strength of the vortex pair in the wake of the following plate (---□---) and the strength of vorticity generated on the following plate (---○---) as functions of the constant external horizontal force F_{xE} for case 1.

Ignoring the viscosity effect, it can be generally believed that when $F_{xE} < 0.1$, the strength of the new vorticity generated by the following plate is less than that of the leading plate.

DATA AVAILABILITY

The data that support the findings of this study are available from the corresponding author upon reasonable request.

REFERENCES

- ¹T. Vicsek and A. Zafeiris, "Collective motion," *Phys. Rep.* **517**, 71–140 (2012).
- ²D. H. Kelley and N. T. Ouellette, "Emergent dynamics of laboratory insect swarms," *Sci. Rep.* **3**, 1073 (2013).
- ³D. Weihs, "Hydromechanics of fish schooling," *Nature* **241**, 290–291 (1973).
- ⁴I. Ashraf, H. Bradshaw, T. T. Ha, J. Halloy, R. Godoy-Diana, and B. Thiria, "Simple phalanx pattern leads to energy saving in cohesive fish schooling," *Proc. Natl. Acad. Sci. U. S. A.* **114**, 9599–9604 (2017).
- ⁵S. J. Portugal, T. Y. Hubel, J. Fritz, S. Heese, D. Trobe, B. Voelkl, S. Hales, A. M. Wilson, and J. R. Usherwood, "Upwash exploitation and downwash avoidance by flap phasing in ibis formation flight," *Nature* **505**, 399–402 (2014).
- ⁶M. Ballerini, N. Cabibbo, R. Candelier, A. Cavagna, E. Cisbani, I. Giardina, V. Lecomte, A. Orlandi, G. Parisi, A. Procaccini, M. Viale, and V. Zdravkovic, "Interaction ruling animal collective behavior depends on topological rather than metric distance: Evidence from a field study," *Proc. Natl. Acad. Sci. U. S. A.* **105**, 1232–1237 (2008).
- ⁷R. W. Whittlesey, S. Liska, and J. O. Dabiri, "Fish schooling as a basis for vertical axis wind turbine farm design," *Bioinspiration Biomimetics* **5**, 035005 (2010).
- ⁸Z. Cui and X. Gao, "Theory and applications of swarm intelligence," *Neural Comput.* **21**, 205–206 (2012).
- ⁹I. D. Couzin, J. Krause, N. R. Franks, and S. A. Levin, "Effective leadership and decision-making in animal groups on the move," *Nature* **433**, 513–516 (2005).
- ¹⁰J. C. Liao, D. N. Beal, G. V. Lauder, and M. S. Triantafyllou, "Fish exploiting vortices decrease muscle activity," *Science* **302**, 1566–1569 (2003).
- ¹¹A. D. Becker, H. Masoud, J. W. Newbolt, M. Shelley, and L. Ristroph, "Hydrodynamic schooling of flapping swimmers," *Nat. Commun.* **6**, 8514 (2015).
- ¹²Z.-R. Peng, H. B. Huang, and X.-Y. Lu, "Hydrodynamic schooling of multiple self-propelled flapping plates," *J. Fluid Mech.* **853**, 587–600 (2018).
- ¹³M. J. Lighthill, *Mathematical Biofluidynamics* (SIAM, Philadelphia, 1975).
- ¹⁴X. J. Zhu, G. W. He, and X. Zhang, "Flow-mediated interactions between two self-propelled flapping filaments in tandem configuration," *Phys. Rev. Lett.* **113**, 238105 (2014).
- ¹⁵S. Ramanarivo, F. Fang, A. Oza, J. Zhang, and L. Ristroph, "Flow interactions lead to orderly formations of flapping wings in forward flight," *Phys. Rev. Fluids* **1**, 071201 (2016).

- ¹⁶L. Dai, G. W. He, X. Zhang, and X. Zhang, "Stable formations of self-propelled fish-like swimmers induced by hydrodynamic interactions," *J. R. Soc. Interface* **15**, 20180490 (2018).
- ¹⁷G. Li, D. Kolomenskiy, H. Liu, B. Thiria, and R. Godoy-Diana, "On the energetics and stability of a minimal fish school," *PLoS One* **14**, e0215265 (2019).
- ¹⁸L. Li, M. Nagy, J. M. Graving, B. C. Joseph, G. M. Xie, and I. D. Couzin, "Vortex phase matching as a strategy for schooling in robots and in fish," *Nat. Commun.* **11**, 5408 (2020).
- ¹⁹Y. Pan and H. B. Dong, "Computational analysis of hydrodynamic interactions in a high-density fish school," *Phys. Fluids* **32**, 121901 (2020).
- ²⁰H. Y. Yu, X.-Y. Lu, and H. B. Huang, "Collective locomotion of two uncoordinated undulatory self-propelled foils," *Phys. Fluids* **33**, 011904 (2021).
- ²¹L. B. Jia and X. Z. Yin, "Passive oscillations of two tandem flexible filaments in a flowing soap film," *Phys. Rev. Lett.* **100**, 228104 (2008).
- ²²L. Ristroph and J. Zhang, "Anomalous hydrodynamic drafting of interacting flapping flags," *Phys. Rev. Lett.* **101**, 194502 (2008).
- ²³S. Kim, W.-X. Huang, and H. J. Sung, "Constructive and destructive interaction modes between two tandem flexible flags in viscous flow," *J. Fluid Mech.* **661**, 511–521 (2010).
- ²⁴Y. J. Chen, J. Ryu, Y. Z. Liu, and H. J. Sung, "Flapping dynamics of vertically clamped three-dimensional flexible flags in a Poiseuille flow," *Phys. Fluids* **32**, 071905 (2020).
- ²⁵B. M. Boschitsch, P. A. Dewey, and A. J. Smits, "Propulsive performance of unsteady tandem hydrofoils in an in-line configuration," *Phys. Fluids* **26**, 051901 (2014).
- ²⁶A. De Rosi, G. Falcucci, S. Ubertini, and F. Ubertini, "Aeroelastic study of flexible flapping wings by a coupled lattice Boltzmann-finite element approach with immersed boundary method," *J. Fluids Struct.* **49**, 516–533 (2014).
- ²⁷N. Gravish, J. M. Peters, S. A. Combes, and R. J. Wood, "Collective flow enhancement by tandem flapping wings," *Phys. Rev. Lett.* **115**, 188101 (2015).
- ²⁸L. F. Cong, B. Teng, and L. Cheng, "Hydrodynamic behavior of two-dimensional tandem-arranged flapping flexible foils in uniform flow," *Phys. Fluids* **32**, 021903 (2020).
- ²⁹T. M. Broering and Y.-S. Lian, "The effect of phase angle and wing spacing on tandem flapping wings," *Acta Mech. Sin.* **28**, 1557–1571 (2012).
- ³⁰S. G. Park and H. J. Sung, "Hydrodynamics of flexible fins propelled in tandem, diagonal, triangular and diamond configurations," *J. Fluid Mech.* **840**, 154–189 (2018).
- ³¹S. Im, S. G. Park, Y. Cho, and H. J. Sung, "Schooling behavior of rigid and flexible heaving airfoils," *Int. J. Heat Fluid Flow* **69**, 224–233 (2018).
- ³²J. W. Newbolt, J. Zhang, and L. Ristroph, "Flow interactions between uncoordinated flapping swimmers give rise to group cohesion," *Proc. Natl. Acad. Sci. U. S. A.* **116**, 2419–2424 (2019).
- ³³A. U. Oza, L. Ristroph, and M. J. Shelley, "Lattices of hydrodynamically interacting flapping swimmers," *Phys. Rev. X* **9**, 041024 (2019).
- ³⁴X. J. Lin, J. Wu, T. W. Zhang, and L. M. Yang, "Self-organization of multiple self-propelling flapping foils: Energy saving and increased speed," *J. Fluid Mech.* **884**, R1 (2020).
- ³⁵J. Ryu, J. M. Yang, S. G. Park, and H. J. Sung, "Phase-mediated locomotion of two self-propelled flexible plates in a tandem arrangement," *Phys. Fluids* **32**, 041901 (2020).
- ³⁶X. J. Lin, J. Wu, T. W. Zhang, and L. M. Yang, "Flow-mediated organization of two freely flapping swimmers," *J. Fluid Mech.* **912**, A37 (2021).
- ³⁷C. W. Reynolds, "Flocks, herds and schools: A distributed behavioral model," *ACM SIGGRAPH Comput. Graphics* **21**, 25–34 (1987).
- ³⁸C. M. Breder, "The locomotion of fishes," *Zoologica* **4**, 159–297 (1926).
- ³⁹C. Lindsey, "Form, function and locomotory habits in fish," in *Fish Physiology Locomotion*, edited by W. Hoar and D. Randall (Academic Press, New York, 1978), Vol. VII.
- ⁴⁰M. Sfakiotakis, D. M. Lane, and J. Davies, "Review of fish swimming modes for aquatic locomotion," *IEEE J. Oceanic Eng.* **24**, 237–252 (1999).
- ⁴¹P. Liao, S. Zhang, and D. Sun, "A dual caudal-fin miniature robotic fish with an integrated oscillation and jet propulsive mechanism," *Bioinspiration Biomimetics* **13**, 036007 (2018).
- ⁴²W. Wang, X. Dai, B. Gheneti, Y. Ding, J. Z. Yu, and G. M. Xie, "Three-dimensional modeling of a fin-actuated robotic fish with multimodal swimming," *IEEE-ASME Trans. Mechatron.* **23**, 1641 (2018).
- ⁴³J. Z. Wu, H. Y. Ma, and M. D. Zhou, *Vortical Flows* (Springer, 2015).
- ⁴⁴L. L. Kang, L. Q. Liu, W. D. Su, and J. Z. Wu, "Minimum-domain impulse theory for unsteady aerodynamic force," *Phys. Fluids* **30**, 016107 (2018).
- ⁴⁵B. S. H. Connell and D. K. P. Yue, "Flapping dynamics of a flag in a uniform stream," *J. Fluid Mech.* **581**, 33–67 (2007).
- ⁴⁶S. Y. Chen and G. D. Doolen, "Lattice Boltzmann method for fluid flows," *Annu. Rev. Fluid Mech.* **30**, 329–329 (1998).
- ⁴⁷S. Succi, *The Lattice Boltzmann Equation for Fluid Dynamics and Beyond* (Oxford University Press, 2001).
- ⁴⁸J. Doyle and E. Desantiago, "Nonlinear analysis of thin-walled structures: Statics, dynamics, and stability. Mechanical engineering series," *Appl. Mech. Rev.* **55**, B92 (2002).
- ⁴⁹C. S. Peskin, "The immersed boundary method," *Acta Numer.* **11**, 479–517 (2002).
- ⁵⁰C. Tang, N. S. Liu, and X.-Y. Lu, "Dynamics of an inverted flexible plate in a uniform flow," *Phys. Fluids* **27**, 073601 (2015).
- ⁵¹R.-N. Hua, L. D. Zhu, and X.-Y. Lu, "Locomotion of a flapping flexible plate," *Phys. Fluids* **25**, 121901 (2013).
- ⁵²W. J. Wang, H. B. Huang, and X.-Y. Lu, "Optimal chordwise stiffness distribution for self-propelled heaving flexible plates," *Phys. Fluids* **32**, 111905 (2020).
- ⁵³A. De Rosi, G. Falcucci, S. Ubertini, and F. Ubertini, "A coupled lattice Boltzmann-finite element approach for two-dimensional fluid-structure interaction," *Comput. Fluids* **86**, 558–568 (2013).
- ⁵⁴A. De Rosi, S. Ubertini, and F. Ubertini, "A comparison between the interpolated bounce-back scheme and the immersed boundary method to treat solid boundary conditions for laminar flows in the lattice Boltzmann framework," *J. Sci. Comput.* **61**, 477–489 (2014).
- ⁵⁵A. De Rosi, S. Ubertini, and F. Ubertini, "A partitioned approach for two-dimensional fluid-structure interaction problems by a coupled lattice Boltzmann-finite element method with immersed boundary," *J. Fluids Struct.* **45**, 202–215 (2014).
- ⁵⁶G. S. Triantafyllou, M. S. Triantafyllou, and M. A. Grosenbaugh, "Optimal thrust development in oscillating foils with application to fish propulsion," *J. Fluids Struct.* **7**, 205–224 (1993).
- ⁵⁷D. Floryan, T. van Buren, C. W. Rowley, and A. J. Smits, "Scaling the propulsive performance of heaving and pitching foils," *J. Fluid Mech.* **822**, 386–397 (2017).
- ⁵⁸J. Zhang, "Footprints of a flapping wing," *J. Fluid Mech.* **818**, 1–4 (2017).
- ⁵⁹G. K. Taylor, "Simple scaling law predicts peak efficiency in oscillatory propulsion," *Proc. Natl. Acad. Sci. U. S. A.* **115**, 8063–8065 (2018).
- ⁶⁰L. L. Kang, L. Russo, R. Tognaccini, J. Z. Wu, and W. D. Su, "Aerodynamic force breakdown in reversible and irreversible components by vortex force theory," *AIAA J.* **57**, 4623 (2019).
- ⁶¹Z. L. Guo, C. G. Zheng, and B. C. Shi, "Discrete lattice effects on forcing terms in the lattice Boltzmann method," *Phys. Rev. E* **65**, 046308 (2002).
- ⁶²C. K. Aidun and J. R. Clausen, "Lattice-Boltzmann method for complex flows," *Annu. Rev. Fluid Mech.* **42**, 439–472 (2010).
- ⁶³D. Yu, R. Mei, and W. Shyy, "A multi-block lattice Boltzmann method for viscous fluid flows," *Int. J. Numer. Methods Fluids* **39**, 99–120 (2002).
- ⁶⁴P. Bhatnagar, E. Gross, and M. Krook, "A model for collision processes in gases. I. Small amplitude processes in charged and neutral one-component systems," *Phys. Rev.* **94**, 511–525 (1954).
- ⁶⁵Y. Cheng and J. Li, "Introducing unsteady non-uniform source terms into the lattice Boltzmann model," *Int. J. Numer. Methods Fluids* **56**, 629–641 (2008).
- ⁶⁶M. Gazzola, M. Argentina, and L. Mahadevan, "Scaling macroscopic aquatic locomotion," *Nat. Phys.* **10**, 758 (2014).